

The fingerprint of binary intermediate mass black holes in globular clusters: supra-thermal stars and angular momentum alignment

M. Mapelli¹, M. Colpi², A. Possenti³ & S. Sigurdsson⁴

¹*S.I.S.S.A., Via Beirut 2 - 4, I-34014 Trieste, Italy; mapelli@sissa.it*

²*Dipartimento di Fisica G. Occhialini, Università di Milano Bicocca, Piazza della Scienza 3. I-20126 Milano, Italy; monica.colpi@mib.infn.it*

³*INAF, Osservatorio Astronomico di Cagliari, Poggio dei Pini, Strada 54, 09012 Capoterra, Italy; possenti@ca.astro.it*

⁴*Department of Astronomy and Astrophysics, The Pennsylvania State University, 525 Davey Lab, University Park, PA 16802; steinn@astro.psu.edu*

23 September 2018

ABSTRACT

We explore the signatures that a binary intermediate mass black hole (IMBH) imprints on the velocity and on the angular momentum of globular cluster stars. Simulating 3-body encounters between a star and a binary IMBH, we find that the binary IMBH generates a family of few hundreds of stars (~ 100 -300) which remain bound to the globular cluster (GC) and have velocity significantly higher than the dispersion velocity. For this reason we term them "supra-thermal" stars. We also notice that, after the interaction, a considerable fraction (55-70%) of stars tend to align their orbital angular momentum with the angular momentum of the binary IMBH, introducing an anisotropy in the angular momentum distribution of cluster stars. We simulate the dynamical evolution of these supra-thermal stars before thermalization, and find that these stars tend to cluster at a distance of few core radii from the GC center. We conclude that the detectability of such signatures appears problematic with present telescopes.

Key words: black hole physics-globular clusters: general-stellar dynamics

1 INTRODUCTION

A number of different observations suggest that large black holes (BHs) may exist in nature, with masses between $20M_{\odot} - 10^4M_{\odot}$. Heavier than the stellar-mass BHs born in core-collapse supernovae ($3M_{\odot} - 20M_{\odot}$; Orosz 2002), these intermediate mass black holes (IMBHs) are expected to form from the direct collapse of very massive stars, or in dense stellar systems through complex dynamical processes. Filling the gap between stellar-mass black holes (BHs) and super-massive black holes (SMBHs), they are of crucial importance in establishing the potential physical link between these two classes.

IMBHs may plausibly have formed in the early universe as remnants of the first generation of metal free stars (Abel, Bryan & Norman 2002; Heger et al. 2003; Schneider et al. 2002). If this is true, IMBHs can participate the cosmic assembly of galaxies and be incorporated in larger and larger units, becoming seeds for the formation of SMBHs (Madau & Rees 2001; Volonteri, Haardt & Madau 2003). IMBH may still be forming in young dense star clusters vulnerable to unstable mass segregation, via collisions of massive stars

(Portegies Zwart 2004; Portegies Zwart et al. 2004; Portegies Zwart & McMillan 2002; Gürkan et al. 2004; Freitag et al. 2005a, 2005b; see van der Marel 2004 for a review). Unambiguous detections of individual IMBHs do not exist yet, but there are observational hints in favor of their existence, from studies of ultra-luminous X-ray sources in nearby star-forming galaxies (Fabbiano 2004; Mushotzky 2004; Miller & Hamilton 2002).

It has also been long suspected that globular clusters (GCs) may hide IMBHs in their cores (Shapiro 1977; Shapiro & Marchant 1978; Marchant & Shapiro 1979, 1980; Duncan & Shapiro 1982; see Shapiro 1985 for a review), despite the fact that their formation root is poorly known: runaway mergers among the most massive stars, at the time of cluster formation, can lead to an IMBH, similarly to what has been conjectured to occur in young dense star clusters (Portegies Zwart et al. 2004; Fregeau et al. 2004). An alternative pathway is based on the idea that IMBHs form later in the evolution of GCs through mergers of stellar-mass BHs. Segregating by dynamical friction in the core, these BHs are captured in binaries that form through dynamical en-

counters with stars and BHs. The picture is that hardening by subsequent interactions with BHs lead them to merge, emitting gravitational waves (Miller & Hamilton 2002). BHs more massive than stellar-mass BHs are thus created. However, the interactions that produce hardening also provide recoil, causing the ejection of BHs (Kulkarni, Hut & McMillan 1993; Sigurdsson & Hernquist 1993; Portegies Zwart & McMillan 2000), but the heaviest black holes may remain, if their mass exceeds a still uncertain value between $\sim 50M_{\odot}$ and $\sim 300M_{\odot}$ (Miller & Hamilton 2002; Colpi, Mapelli & Possenti 2003; Gultekin, Miller & Hamilton 2004).

At present, optical observations of GCs hint in favor of the existence of IMBHs. In particular Gebhardt, Rich & Ho (2002) suggest the presence of a $2_{-0.8}^{+1.4} \times 10^4 M_{\odot}$ IMBH, to explain the kinematics and the surface brightness profile of the globular cluster G1 in M31. Gerssen et al. follow the same method to indicate the possible presence of a $1.7_{-1.7}^{+2.7} \times 10^3 M_{\odot}$ IMBH in the galactic globular cluster M15 (Gerssen et al. 2002, 2003). These indications are still controversial, as Baumgardt et al (2003a, 2003b) showed that both the measurements of M15 and those of G1 can be explained with a central concentration of compact objects (neutron stars and white dwarfs) instead of the presence of a massive black hole. However, a more recent paper by Gebhardt, Rich & Ho (2005) further supports the hypothesis of an IMBH in G1. In addition, there has been some claim of the existence of rotation in the core of a few GCs (Gebhardt et al. 1995; Gebhardt et al. 1997; Gebhardt et al. 2000) suggesting the presence of a steady source of angular momentum in their cores.

Radio observations can also help in discovering concentrations of under-luminous matter in the core of GCs, thanks to the presence of millisecond pulsars that can probe the underlying gravitational field of the cluster. Currently, there are more than 100 known millisecond pulsars in GCs (Possenti 2003; Ransom et al. 2005; Camilo & Rasio 2005) and some show large and negative period derivatives. This is an important peculiarity, because millisecond pulsars spin down intrinsically due to magnetic braking. Negative period derivatives come from the variable Doppler shift caused by the acceleration of the pulsar in the gravitational field of the cluster itself (Phinney 1993). When these negative period derivatives can be ascribed solely to the gravitational field of the cluster, these pulsars place a lower limit on the mass enclosed inside their projected distance from the globular cluster center.

Two pulsars in M15, at 1" from the cluster center were found (Phinney 1993) with negative values of their period derivatives, consistent with the mass distribution implied by the stellar kinematics. The recent discovery by D'Amico et al. (2002) of two accelerated pulsars in NGC 6752 at 6" and 7" from the center has highlighted the presence of about $2 \times 10^3 M_{\odot}$ of under-luminous matter in the core of the cluster (Ferraro et al. 2003a), making NGC 6752 a special target for the search of an IMBH. NGC 6752 is interesting also because it hosts two pulsars in its halo. PSR-A is a millisecond pulsar in a binary system with a white dwarf (Bassa et al. 2003; Ferraro et al. 2003b), located at 3.3 half mass radii away: it is the farthest pulsar ever observed in a cluster. Colpi, Possenti & Gualandris (2002), and Colpi, Mapelli & Possenti (2003, 2004) have suggested that this pulsar has been propelled in the halo due to a dynamical interaction with a binary IMBH.

In modeling the gravitational encounter, Colpi, Mapelli & Possenti (2003) found that a $(50-200, 10) M_{\odot}$ binary IMBH is the preferred target for imprinting the large kick to the pulsar. Colpi et al. (2005) shortly reviewed the dynamical effects that a binary IMBH would imprint on cluster stars.

Considering all the recent hints provided by optical and radio observations, we explore, in this paper, a new way to unveil a binary IMBH in a GC, previously overlooked, that exploits the dynamical fingerprint left by a binary IMBH on cluster stars. In particular we like to address a number of questions: (i) What signature does a binary IMBH imprint on cluster stars? Are the stars heated during the scattering process still remaining bound to the cluster? (ii) Is there direct transfer of angular momentum from the binary IMBH to the stars to produce some degree of alignment, given the large inertia of the BHs? (iii) Are prograde or retrograde orbits equally scattered?

In this paper, we simulate 3-body encounters of cluster stars with a binary IMBH, studying the energy and angular momentum exchange, and reconstructing the trajectories of those stars that are scattered away from equilibrium by the binary IMBH. In Section 2 we outline the method used to simulate 3-body encounters between a binary IMBH and the cluster stars. In Section 3 we present our main results: the formation, in a GC hosting a binary IMBH, of a population of high velocity (bound) stars (that we call "supra-thermal stars"), which tend to align their orbital angular momentum with that of the binary IMBH. In Section 4 we investigate on the expected number of these supra-thermal stars. In particular, we use an upgraded version of the code presented in Sigurdsson & Phinney (1995) to follow the dynamical evolution of these supra-thermal stars inside a GC model which reproduces the characteristics of NGC 6752. This study allows us to put some constraint on the detectability of this family of high velocity stars. Section 5 contains our conclusions.

2 THE SIMULATIONS

We simulated 3-body encounters involving a binary IMBH (composed of two BHs of mass M_1 and M_2) and a cluster star of mass $m = 0.5 M_{\odot}$. The dynamics of the encounter is followed solving the equations of motion with a numerical code based on a Runge-Kutta fourth order integration scheme with adaptive stepsize and quality control (explained in Colpi, Mapelli & Possenti 2003, hereafter CMP). For the target binary IMBH we considered an interval of masses between $60 M_{\odot}$ up to $210 M_{\odot}$. These are the favored masses of the hypothetical binary IMBH in NGC 6752. The binary has semi-major axis a of 1, 10, 100, and 1000 AU and eccentricity¹ $e = 0.7$, which is nearly the average binary eccentricity in statistical equilibrium (Hills 1975). The set of models is described in Table 1.

The initial conditions, that are Monte Carlo generated as in CMP, are sampled using the prescriptions indicated in Hut & Bahcall (1983). In particular, the relative velocity u^{in}

¹ We have repeated select simulations for different values of the eccentricity and find only minor quantitative differences ($\lesssim 10\%$) in our results.

is distributed homogeneously between $8.5 - 11 \text{ km s}^{-1}$ (according to the value of stellar velocity dispersion measured in NGC 6752 which is our reference cluster; Dubath, Meylan & Mayor 1997), and the impact parameter b is drawn at random from a probability distribution uniform in b^2 and in a range going from 0 to a truncation value b_{max} . The truncation value b_{max} is chosen by requiring that the simulations include all the encounters with non-negligible energetic exchange, i.e. with outgoing velocities of the interacting star significantly higher than the initial velocity (see Appendix A for a discussion of our choices of the impact parameter ranges). The three orientation angles and the phase of the binary are generated as indicated in Table 1 and 2 of Hut & Bahcall (1983). We initiate (terminate) integration when the distance between the incoming (outgoing) star and the center of mass of the binary is comparable to the radius of gravitational influence of the IMBHs ($r_a \sim 2G(M_1 + M_2)/\sigma^2$, where σ is the 1-D stellar dispersion velocity). At the start of each simulation, we place the binary BH and the single star on their respective hyperbolic trajectories.

At the end of every scattering experiment we store the final binding energy E_{BH}^{fin} and angular momentum \mathbf{J}_{BH}^{fin} of the binary IMBH, together with the velocity at infinity (or post-encounter asymptotic velocity) u^{fin} , defined as the velocity of the interacting star after the encounter, extrapolated at infinity, and the angular momentum \mathbf{J}_{*}^{fin} of the interacting star. In this paper we want, in particular, to quantify the mean change in the absolute value J_* of the vector \mathbf{J}_* and the extent of alignment of \mathbf{J}_* in the direction of \mathbf{J}_{BH} .

3 RESULTS

3.1 Supra-thermal stars

We find that a sizable number of high velocity stars is created, under certain conditions, that may highlight the presence of an IMBH in the cluster. These stars gain kinetic energy and an excess velocity relative to the mean, remaining bound to the cluster. In Table 3 we give the fraction of bound stars, defined as those having a final velocity lower than the escape velocity from the core $\sim 35-40 \text{ km s}^{-1}$, and the fraction of high velocity or *supra-thermal* stars, defined as having a post-encounter asymptotic (or "at infinity") speed between 20 and 40 km s^{-1} . Depending on the characteristics of the binary IMBH, these stars can account for $\lesssim 50\%$ of all stars that have experienced an encounter.

Figure 1 shows the distribution of the velocity at infinity of stars scattering off a binary IMBH, for cases D1, D2, D3 and D4 (in Table 1). The shaded area indicates the strip of supra-thermal stars. The mean values of the speed at infinity u^{fin} and of the fractional binding energy exchange $\langle \Delta E_{BH}/E_{BH}^{fin} \rangle = \langle (E_{BH}^{fin} - E_{BH}^{in})/E_{BH}^{in} \rangle$ are given in Table 2 together with the dimensionless factor ξ_E , defined by:

$$\langle \Delta E_{BH}/E_{BH}^{fin} \rangle = \xi_E [m/(M_1 + M_2)]. \quad (1)$$

As illustrated in Figure 1, dynamical encounters widen the velocity distribution of the stars. This effect is particularly severe when the binary is hard, having a higher binding energy which becomes available in the interaction. ξ_E clusters

around values between 0.6 and 4, and shows a maximum declining as the binary becomes extremely hard. This explains why case D1 has a peak velocity at infinity smaller than case D2 corresponding to a less hard binary (see Table 2). We tried to fit the behavior of ξ_E , as a function of the orbital separation a , with a parabola. We obtained $\xi_E = b \text{Log}^2(a) + c \text{Log}(a) + d$ for $b=-1.2495$, $c=3.8615$, $d=0.958$; this fit is only an approximation, since we have few numerical points (Fig. 2). It is interesting to notice that for $a = 1 \text{ AU}$ ξ_E is lower than for wider binaries. This does not represent a violation of the first statement of Heggie's law (i.e. that hard binaries tend to become more energetic, Heggie 1975; Hills 1990); in fact all our hard binaries become harder and harder. But a ξ_E decreasing for $a < 10 \text{ AU}$ seems in partial disagreement with the second statement of Heggie's law, for which the hardening rate of the binaries is "approximately independent of their binding energy" (Heggie 1975). This difference is the result of a different approach with respect to that followed by Heggie. In fact, we are treating very massive binaries with respect to the incoming star, and such binaries require very large maximum impact parameters, nearly independently of their semi-major axis, to include in our simulations all the interactions which have significant energy exchange (i.e. $\Delta E_{BH}/E_{BH}^{fin} > 10^{-3}$), corresponding to post-encounter asymptotic velocities of the star in the supra-thermal range (see Appendix A for a complete discussion).

In Figure 1, case D1 and D3 give the highest number of supra-thermal stars among the different runs. These supra-thermal stars are the ones that have also acquired a sizable fraction of the orbital angular momentum of the binary IMBH. Thus in scattering off the binary IMBH they are preferentially launched in a halo orbit, inside the cluster. Their detection (discussed in § 4) would be the sign of an IMBH hidden in the cluster.

3.2 Angular Momentum Transfer and Alignment

An interesting question to address is whether and how the orbital angular momentum of the binary IMBH couples to the star after a close gravitational encounter. The BHs can be sufficiently massive and the orbit be sufficiently wide that the orbital angular momentum of the binary exceeds that of the incoming star. In this case a direct transfer of orbital angular momentum can occur. The star coming close to the binary IMBH can be dragged into corotation, i.e. the star can emerge after the encounter with an angular momentum nearly aligned with the binary IMBH.

If we denote with $\mu = M_1 M_2 / (M_1 + M_2)$ the reduced mass of the binary hosting the two BHs, the total angular momentum of the system is

$$\mathbf{J} = \mathbf{J}_{BH}^{in} + \mathbf{J}_{*}^{in} = \mu \sqrt{a G (M_1 + M_2)} \mathbf{z} + b u^{in} \left[\frac{m(M_1 + M_2)}{M_1 + M_2 + m} \right] \mathbf{z}' \quad (2)$$

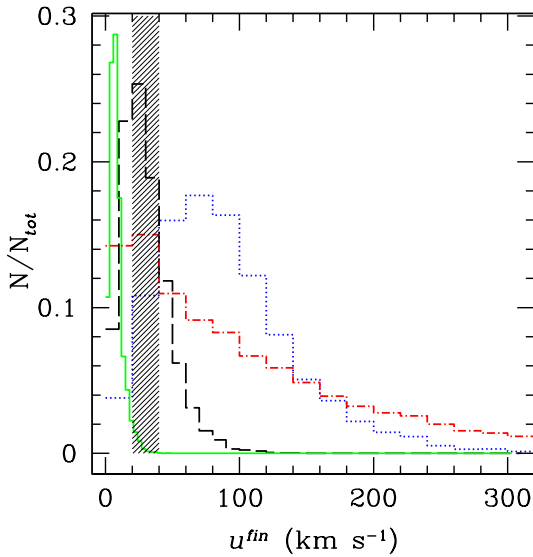
where \mathbf{z} and \mathbf{z}' are the unit vectors indicating respectively the directions of \mathbf{J}_{BH}^{in} and \mathbf{J}_{*}^{in} . Angular momentum transfer from the binary to the interacting star and partial alignment become important when $J_{BH}^{in} \gg J_{*}^{in}$, i.e., when

$$\frac{\mu}{b u^{in} m} \sqrt{(M_1 + M_2) a G} \gg 1. \quad (3)$$

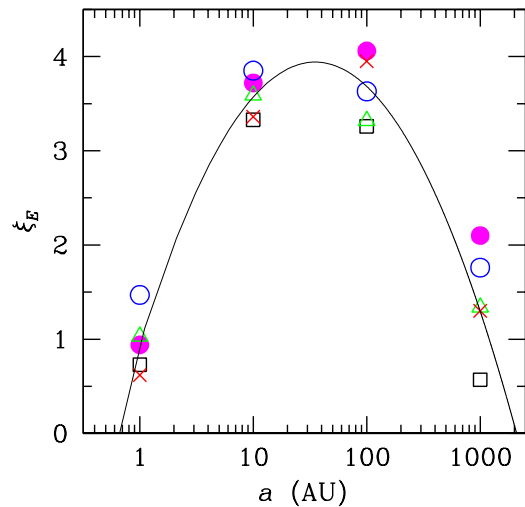
Our experiment confirms this fact. Figure 3 (solid lines)

Table 1. Initial Parameters.

	M_1^a	M_2^a	Semi-major axis (a) ^b	Range of impact parameters ^b	Number of simulations
CASE A1	50	10	1	0-60	5000
CASE A2	50	10	10	0-60	10000
CASE A3	50	10	100	0-100	10000
CASE A4	50	10	1000	0-1000	10000
CASE B1	50	50	1	0-100	5000
CASE B2	50	50	10	0-100	5000
CASE B3	50	50	100	0-100	5000
CASE B4	50	50	1000	0-1000	5000
CASE C1	100	10	1	0-100	5000
CASE C2	100	10	10	0-100	5000
CASE C3	100	10	100	0-100	5000
CASE C4	100	10	1000	0-1000	5000
CASE D1	100	50	1	0-100	5000
CASE D2	100	50	10	0-100	5000
CASE D3	100	50	100	0-100	5000
CASE D4	100	50	1000	0-1000	5000
CASE E1	200	10	1	0-100	5000
CASE E2	200	10	10	0-100	5000
CASE E3	200	10	100	0-100	5000
CASE E4	200	10	1000	0-1000	5000

^a In units of the solar mass.^b In Astronomical Units.**Figure 1.** Post-encounter asymptotic velocity distributions of the cluster star in the case D1 (dotted-dashed line), D2 (dotted line), D3 (dashed line), D4 (solid line). The shaded area refers to the supra-thermal stars. On the y-axis the number of cases for each bin is normalized to the total number of resolved runs (N_{tot}).

shows the post-encounter distribution of J_* for cases D2, D3 and D4. It is compared with the distribution of J_* of the incoming stars (dashed lines) to show that the binary IMBH transfers angular momentum to the stars widening the distribution of J_* . Table 2 contains the averaged value

**Figure 2.** $\xi_E \equiv [(M_1 + M_2)/m]\langle \Delta E_{BH}/E_{BH}^{in} \rangle$ as a function of the orbital separation a for all the considered cases. A1, A2, A3 and A4 are represented by open triangles; B1, B2, B3 and B4 by crosses; C1, C2, C3 and C4 by open squares; D1, D2, D3 and D4 by filled circles; E1, E2, E3 and E4 by open circles. The solid line indicates a parabolic fit $b \log^2(a) + c \log(a) + d = \xi_E(a)$, where $b=-1.2495$, $c=3.8615$, $d=0.958$.

of the fractional angular momentum increase (in modulus) $\langle \Delta J_*/J_*^{in} \rangle$ for the complete series of runs. $\langle \Delta J_*/J_*^{in} \rangle$ is large and exceeds unity in correspondence to the runs where

Table 2. Final velocities and angular momentum exchanges.^a

	u^{fin} ^b	$\langle \frac{\Delta J}{J_*^{in}} \rangle^c$	$\frac{\Delta J}{J_*^{in}}$ ^d	$\langle \frac{\Delta E_{BH}}{E_{BH}^{in}} \rangle^e$	ξ_E^f
CASE A1	$12.5^{+95.0}_{-10.0}$	$0.056^{+14.40}_{-0.054}$	$0.025^{+0.100}_{-0.100}$	$0.0086^{+0.4520}_{-0.0073}$	1.03
CASE A2	$37.0^{+35.0}_{-30.0}$	$0.630^{+8.24}_{-0.592}$	$0.175^{+1.150}_{-0.850}$	$0.0299^{+1.1032}_{-0.0186}$	3.59
CASE A3	$12.5^{+10.0}_{-10.0}$	$1.12^{+1.82}_{-1.13}$	$0.725^{+2.200}_{-1.400}$	$0.0277^{+1.0363}_{-0.0191}$	3.32
CASE A4	$7.5^{+2.0}_{-3.0}$	$0.155^{+30.330}_{-0.228}$	$0.025^{+0.350}_{-0.500}$	$0.0112^{+0.0309}_{-0.0199}$	1.34
CASE B1	$12.5^{+75.0}_{-12.5}$	$0.037^{+7.980}_{-0.037}$	$0.005^{+0.020}_{-0.005}$	$0.0031^{+0.1778}_{-0.0030}$	0.62
CASE B2	$67.5^{+60.0}_{-55.0}$	$0.317^{+31.840}_{-0.346}$	$0.025^{+0.65}_{-0.55}$	$0.0168^{+0.2621}_{-0.0109}$	3.36
CASE B3	$17.5^{+25.0}_{-15.0}$	$1.994^{+145.935}_{-1.456}$	$0.325^{+2.850}_{-1.100}$	$0.0198^{+0.2255}_{-0.0134}$	3.95
CASE B4	$8.5^{+3.0}_{-6.0}$	$0.197^{+17.279}_{-0.259}$	$-0.0255^{+0.550}_{-0.400}$	$0.0065^{+0.0150}_{-0.0073}$	1.30
CASE C1	$12.5^{+60.0}_{-10.0}$	$0.020^{+5.726}_{-0.020}$	$0.005^{+0.010}_{-0.005}$	$0.0033^{+0.7152}_{-0.0032}$	0.73
CASE C2	$32.5^{+40.0}_{-25.0}$	$0.154^{+0.891}_{-0.284}$	$0.075^{+0.550}_{-0.550}$	$0.0151^{+0.4422}_{-0.0095}$	3.33
CASE C3	$12.5^{+10.0}_{-10.0}$	$0.876^{+1.639}_{-1.135}$	$0.520^{+3.200}_{-1.040}$	$0.0148^{+0.5524}_{-0.0098}$	3.26
CASE C4	$5.9^{+2.5}_{-3.1}$	$0.212^{+21.888}_{-0.255}$	$0.025^{+0.500}_{-0.500}$	$0.00261^{+0.00911}_{-0.00773}$	0.57
CASE D1	$30.0^{+160.0}_{-30.0}$	$0.062^{+12.175}_{-0.059}$	$0.005^{+0.090}_{-0.050}$	$0.0031^{+0.1054}_{-0.0027}$	0.94
CASE D2	$75.0^{+70.0}_{-60.0}$	$0.205^{+0.703}_{-0.623}$	$0.225^{+0.850}_{-1.000}$	$0.0124^{+0.1679}_{-0.0078}$	3.72
CASE D3	$22.5^{+30.0}_{-20.0}$	$2.911^{+7.894}_{-1.801}$	$1.235^{+3.780}_{-1.890}$	$0.0135^{+0.0348}_{-0.0090}$	4.06
CASE D4	$7.0^{+6.0}_{-6.0}$	$0.384^{+1.243}_{-0.512}$	$0.185^{+1.050}_{-0.840}$	$0.0070^{+0.7796}_{-0.0065}$	2.10
CASE E1	$27.5^{+105.0}_{-25.0}$	$0.025^{+7.087}_{-0.024}$	$0.005^{+0.050}_{-0.030}$	$0.0035^{+0.7193}_{-0.0027}$	1.47
CASE E2	$32.5^{+45.0}_{-25.0}$	$0.429^{+28.250}_{-0.381}$	$0.065^{+0.540}_{-0.420}$	$0.0092^{+0.6392}_{-0.0058}$	3.85
CASE E3	$13.5^{+12.0}_{-12.0}$	$1.212^{+3.718}_{-0.881}$	$0.675^{+1.350}_{-1.700}$	$0.0086^{+0.6697}_{-0.0060}$	3.63
CASE E4	$6.5^{+3.0}_{-5.0}$	$0.395^{+50.771}_{-0.347}$	$0.075^{+0.450}_{-0.400}$	$0.0042^{+0.0191}_{-0.0067}$	1.76

^a We consider both bound and ejected stars. Only unresolved encounters are neglected in this Table.

^b In units of km s^{-1} . Peak value of the velocity at infinity of the star cluster. The dispersion around the peak value is calculated considering those values which contain 50% of the total area descending from the peak.

^c $\Delta J \equiv (J_*^{fin} - J_*^{in})$, where J_*^{in} and J_*^{fin} represent respectively the modulus of the initial and the final angular momentum of the cluster star. $\langle \frac{\Delta J}{J_*^{in}} \rangle$ is the mean value of the variation of the absolute value of the angular momentum of the cluster star, normalized to its initial value J_*^{in} . The dispersion around the mean value is calculated considering those values which contain 34% of the total area in the left and right wings, respectively.

^d $\frac{\Delta J}{J_*^{in}}$ is the peak value of $\frac{\Delta J}{J_*^{in}}$. The dispersion around the peak value is calculated considering those values which contain 50% of the total area descending from the peak.

^e $\langle \frac{\Delta E_{BH}}{E_{BH}^{in}} \rangle$ is the mean value of the variation of the binding energy of the binary IMBH, normalized to its initial binding energy E_{BH}^{in} .

The dispersion around the mean value is calculated considering those values which contain 34% of the total area in the left and right wings, respectively.

^f ξ_E represents the hardening factor and is given by $\xi_E \equiv \frac{M_1+M_2}{m} \langle \frac{\Delta E_{BH}}{E_{BH}^{in}} \rangle$ (CMP 2003).

the bulk of the supra-thermal stars are produced. It has a non monotonic trend with the hardness of the binary: a harder binary has little excess of angular momentum in its initial state relative to that of the incoming star; so the efficiency of angular momentum transfer reduces. A less hard binary (having a larger J_{BH}^{in}) is also less efficient, since it does not alter much the post-encounter asymptotic velocity.

We can further quantify the importance of angular momentum transfer from the binary to the star, by computing the fraction of stars which increase J_* after an interaction; this is given in the last column of Table 4. The fraction of stars that do so, over the total (in the sample of the bound stars), is significantly high: it is above 70% in many cases.

Is alignment induced in the scattering process? In Table 4 we compare the percentage of bound stars which were corotating (i.e. for which the scalar product between their angular momentum and the angular momentum of the bi-

nary is positive, that is $\mathbf{J}_* \cdot \mathbf{J}_{BH} > 0$) before the 3-body interaction with the percentage of those stars which are corotating after the 3-body interaction. Whereas the fraction of corotating stars before the interaction is $\sim 50\%$ (as one can expect given the initial sampling of the data), the fraction of corotating stars after the interaction is often over 60%, indicating a tendency of stars to align their angular momentum with that of the binary IMBH. This tendency is greater if the binary has a big reduced mass (cases with $M_1 = 100$, $M_2 = 50 M_\odot$ and with $M_1 = 50$, $M_2 = 50 M_\odot$) and if the binary is moderately hard (i.e. its orbital separation is neither too small, because in this case J_{BH}^{in} is comparable with J_*^{in} , nor too large, since in this case the binary would be too soft, and so the kinetic energy exchange would be negligible). In case D3 the bound stars which after the interaction are corotating with the binary are $\sim 70\%$. This means that we can observe a family of supra-thermal stars

Table 3. Statistics of the Outgoing States.

	Bound stars (%)	Ejections (%)	Unresolved Encounters (%) ^a	Supra-thermal stars (%) ^b
CASE A1	45.02	53.12	1.86	21.46
CASE A2	51.32	47.10	1.58	35.56
CASE A3	97.60	1.65	0.75	17.23
CASE A4	99.98	0.00	0.02	0.06
CASE B1	53.78	43.44	2.78	13.12
CASE B2	21.12	77.90	0.98	15.58
CASE B3	83.36	16.30	0.34	43.36
CASE B4	99.96	0.00	0.04	0.36
CASE C1	60.46	34.82	4.72	15.10
CASE C2	51.30	45.58	3.12	35.24
CASE C3	95.56	1.80	2.64	17.22
CASE C4	99.86	0.00	0.14	0.01
CASE D1	28.04	67.84	4.12	14.38
CASE D2	14.44	84.18	1.38	10.68
CASE D3	75.20	24.32	0.48	44.04
CASE D4	99.84	0.04	0.12	3.46
CASE E1	27.60	62.54	9.86	17.86
CASE E2	45.84	47.42	6.74	31.54
CASE E3	88.68	2.36	8.96	18.42
CASE E4	98.48	0.02	1.50	0.38

^a We define unresolved interactions those runs where the separation between the star and the binary IMBH never exceeds 30 a after 10^8 time steps.

^b We define supra-thermal stars those with velocities at infinity comprised between 20 and 40 km s⁻¹.

Table 4. Statistics for bound stars^a.

	Corot _{in} (%) ^b	Corot _{fin} (%) ^c	More aligned stars (%) ^d	J _* ^{fin} > J _* ⁱⁿ (%) ^e
CASE A1	40	42	52	64
CASE A2	47	59	61	72
CASE A3	49	68	65	87
CASE A4	50	51	50	55
CASE B1	46	46	50	59
CASE B2	57	63	53	64
CASE B3	50	58	56	83
CASE B4	50	58	55	58
CASE C1	46	46	51	59
CASE C2	45	49	58	64
CASE C3	49	62	64	88
CASE C4	50	52	51	59
CASE D1	40	40	51	64
CASE D2	55	60	52	71
CASE D3	51	70	62	95
CASE D4	50	69	63	71
CASE E1	40	40	50	61
CASE E2	42	45	60	65
CASE E3	48	53	61	92
CASE E4	50	54	59	63

^a In this Table we consider only the stars which after the interaction with the binary remain bound to the cluster.

^b Percentage (respect to the total of bound stars) of stars which, before the interaction, are corotating with the binary (i.e. for which the scalar product between their angular momentum and the angular momentum of the binary is positive).

^c Percentage (respect to the total of bound stars) of stars which, after the interaction, are corotating with the binary, independently from the initial orientation of their angular momentum.

^d Percentage of bound stars which, after the encounter, reduce the angle between their angular momentum and that of the binary.

^e Percentage of bound stars which, after the encounter, increase the absolute value of their angular momentum.

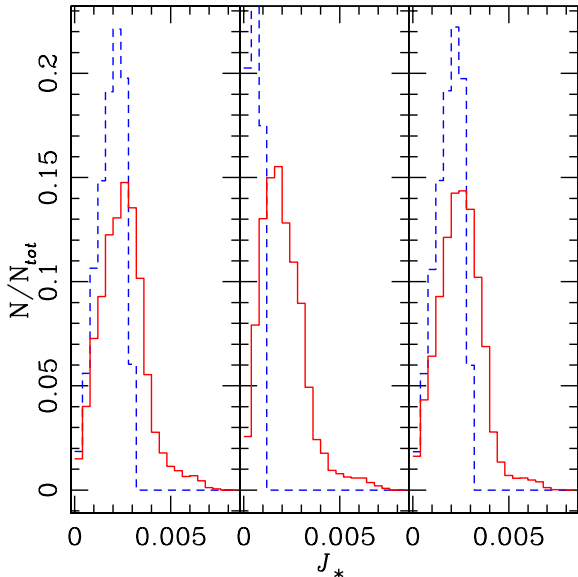


Figure 3. Angular momentum distribution of the cluster star in the case D2 (left panel), D3 (central panel), D4 (right panel). The angular momenta are in dimensionless units (i.e. normalized to the length, mass and time scales). *Dashed line* indicates the initial angular momentum distribution, *solid line* indicates the post-encounter angular momentum distribution. Evidence of angular momentum transfer from the binary to the cluster star occurs when the binary has an semi-major axis of 100 AU (case D3); while the softest binary (case D4, $a=1000$ AU) is the least efficient from this point of view. On the y-axis the number of cases for each bin is normalized to the total number of resolved runs (N_{tot}).

which have an anisotropy in their orbital angular momentum relative to the center of the cluster, 70% of them rotating in one direction and the remaining 30% rotating in the other. Obviously, we have to take into account that orbits initially are isotropically distributed and that we observe them in projection; then the detection of this phenomenon is not so immediate.

Table 4 indirectly shows also another interesting effect. The first column indicates that generally less than 50% of the initially corotating stars remain bound to the cluster, while the post-encounter percentage of corotating stars is more than 50%. This means not only that a fraction of initially counter-rotating stars becomes corotating, but also that an initially corotating star is more easily ejected from the cluster than a counter-rotating star. This fact can be intuitively explained considering that, when a counter-rotating star interacts with the binary, its relative velocity with respect to the lighter BH is higher than in the case of a corotating star, and, then, the cross section is lower.

To better constrain orbit alignment in the direction of \mathbf{J}_{BH} , we considered separately orbits which before the encounter (as initial condition) were corotating (Table 5) and orbits which before the encounter were counterrotating (Table 6). For both we investigated the final distributions, and in particular we compared the fraction of stars initially corotating which after the interaction remain corotating (Table 5, 2nd column) with the fraction of stars initially counterrotating

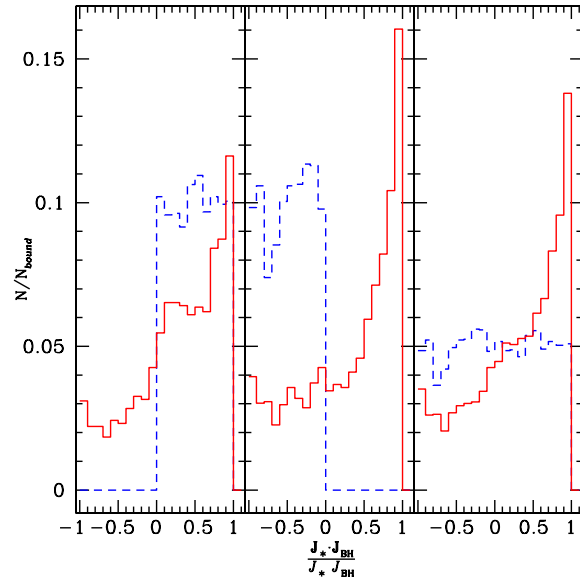


Figure 4. The histograms show the distribution of $\frac{J_* \cdot J_{BH}}{J_* J_{BH}}$ for the case D3 ($M_1 = 100 M_\odot$, $M_2 = 50 M_\odot$, $a = 100$ AU). *Solid line* indicates the distribution after the encounter; *dashed line* indicates the distribution before the encounter. The left panel represents the distribution of $\frac{J_* \cdot J_{BH}}{J_* J_{BH}}$ for bound stars which before the encounter were corotating, the central panel the distribution for bound stars which before the encounter were counterrotating and the right panel the sum of the two distribution, i.e. the distribution for all the stars which after the encounter remain bound to the cluster. On the y-axis the number of cases for each bin is normalized to the total number of bound stars (N_{bound}).

tating which after the interaction become corotating (Table 6, 2nd column). We found that most (at least 70%) of the initially corotating stars remain corotating, even if during very energetic interactions -with the hardest binaries- the star tends to forget its initial angular momentum orientation (case D2). In contrast, a high percentage of initially counterrotating stars becomes corotating, flipping their angular momentum. The combination of these two tendencies (i.e. the tendency to remain corotating for initially corotating stars and the tendency to become corotating for initially counterrotating stars) provides the strongest evidence of an alignment between \mathbf{J}_{BH}^{in} and \mathbf{J}_*^{in} after the interaction (Fig. 4). In Fig. 5 we give a complete overview of the cases considered.

4 DETECTING SUPRA-THERMAL STARS

We want now to estimate how many supra-thermal stars are produced by interactions with a binary IMBH and if they are observable with present instrumentation.

4.1 Estimating the number of supra-thermal stars

Since supra-thermal stars have excess kinetic energy and angular momentum, they are not in thermodynamic equilibrium with respect to the rest of the cluster. Thus, two-body relaxation will try to obliterate such anisotropies. Friction

Table 5. Statistics for initially corotating bound stars^a.

	Corot _{fin} (%) ^b	Counterrot _{fin} (%) ^c	More aligned stars (%) ^d	J _* ^{fin} > J _* ⁱⁿ (%) ^e
CASE A1	93	7	49	70
CASE A2	77	23	44	77
CASE A3	79	21	48	90
CASE A4	82	18	42	53
CASE B1	97	3	50	63
CASE B2	67	33	34	67
CASE B3	60	40	35	84
CASE B4	62	38	33	61
CASE C1	98	2	50	62
CASE C2	81	19	46	73
CASE C3	86	14	48	91
CASE C4	86	14	45	60
CASE D1	92	8	50	68
CASE D2	65	35	31	67
CASE D3	72	28	41	93
CASE D4	75	25	43	71
CASE E1	94	6	48	63
CASE E2	86	14	48	73
CASE E3	96	4	35	95
CASE E4	94	6	53	70

^a In this Table we consider only the stars which before the interaction were corotating.

^b Percentage (respect to the total of initially corotating bound stars) of stars which, after the interaction, remain corotating with the binary.

^c Percentage (respect to the total of initially corotating bound stars) of stars which, after the interaction, become counterrotating respect to the binary.

^d Percentage (respect to the total of initially corotating bound stars) of stars which, after the encounter, reduce the angle between their angular momentum and that of the binary.

^e Percentage of bound stars (respect to the total of initially corotating bound stars) which, after the encounter, increase the absolute value of their angular momentum.

will return them to the core where they become unrecognizable, unless some memory of the angular momentum alignment (e.g. Section 3.2) is retained during the relaxation process.

The existence of supra-thermal stars requires:

- (i) the survival of the IMBH as a binary in the cluster core;
- (ii) the persistence of the supra-thermal stars in the GC halo.

We can investigate these questions through a comparison between relevant timescales. The first timescale to consider is the hardening time of the binary IMBH (Quinlan 1996), given the stellar number density in the core n and the binary separation a

$$t_{hard} = \frac{\sigma}{2\pi a \xi_E G m n} \quad (4)$$

The second relevant timescale is the relaxation time at the half mass radius

$$t_{rh} = \frac{0.14N}{\ln(0.4N)} \left(\frac{r_h^3}{GM} \right)^{1/2} \quad (5)$$

where N and M are respectively the number of stars and the total mass of the cluster. In Figure 6 we compare the two timescales for $\sigma = 8.5 \text{ km s}^{-1}$, $\xi_E \sim 1$ (see Table 2) and $n = 10^5 \text{ stars pc}^{-3}$. This plot shows that, when the binary is not very hard, i.e., when $a > 4 \text{ AU}$, the harden-

ing time is shorter than the half-mass relaxation time. This implies that we can simultaneously observe all the supra-thermal stars in the halo for a time comparable to t_{rh} with no dilution. On the other hand, when the binary has orbital separation $a \leq 4 \text{ AU}$, t_{rh} is shorter than t_{hard} , and, then, we can not simultaneously observe all the produced supra-thermal stars in the halo, a part of them being already thermalized. However, this effect is balanced by the fact that the binary remains in this very hard configuration for most of its life, and, therefore, we can observe a considerable fraction ($\sim 60\%$) of the total number of supra-thermal stars even when the binary is very hard ($a \leq 4 \text{ AU}$). For completeness, we also considered a third timescale: the gravitational wave timescale, t_{gw} , i.e. the characteristic time for a binary IMBH to coalesce due to gravitational wave emission. When this timescale, defined as (Peters 1964; Quinlan 1996)

$$t_{gw} = \frac{5}{256} \frac{c^5 a^4 (1 - e^2)^{7/2}}{G^3 M_1 M_2 (M_1 + M_2)}, \quad (6)$$

becomes shorter than t_{hard} , the binary would shrink, due to gravitational wave emission, at a rate shorter than what we expected from t_{hard} . Figure 6 shows the timescale t_{gw} computed for a constant eccentricity $e = 0.7$ (the initial eccentricity we chose for our runs) and for the range of masses considered in this paper. We expect that the assumption of

Table 6. Statistics for initially counterrotating bound stars^a.

	Corot _{fin} (%) ^b	Counterrot _{fin} (%) ^c	More aligned stars (%) ^d	J _* ^{fin} > J _* ⁱⁿ (%) ^e
CASE A1	7	93	54	60
CASE A2	43	57	75	69
CASE A3	57	43	81	85
CASE A4	21	79	58	57
CASE B1	3	97	49	57
CASE B2	57	43	79	60
CASE B3	56	44	77	82
CASE B4	55	45	79	55
CASE C1	34	66	52	57
CASE C2	23	76	68	57
CASE C3	39	61	79	84
CASE C4	17	83	57	58
CASE D1	6	94	52	61
CASE D2	54	46	78	76
CASE D3	67	33	84	97
CASE D4	62	38	83	71
CASE E1	5	95	52	59
CASE E2	15	85	69	59
CASE E3	13	87	85	90
CASE E4	15	85	65	57

^a In this Table we consider only the stars which before the interaction were counterrotating.

^b Percentage (respect to the total of initially counterrotating bound stars) of stars which, after the interaction, become corotating with the binary.

^c Percentage (respect to the total of initially counterrotating bound stars) of stars which, after the interaction, remain counterrotating respect to the binary.

^d Percentage (respect to the total of initially counterrotating bound stars) of stars which, after the encounter, reduce the angle between their angular momentum and that of the binary.

^e Percentage of bound stars (respect to the total of initially counterrotating bound stars) which, after the encounter, increase the absolute value of their angular momentum.

constant eccentricity is correct for star-binary IMBH interactions, since, when $M_1 + M_2 \gg m$, the binary eccentricity suffers very small changes. We also checked whether this assumption is correct on the basis of our simulations. We found that the mean eccentricity e of the binary IMBH after a 3-body encounter is always 0.70, with a very narrow spread (the standard deviation σ being always $1 - 5 \times 10^{-2}$), and the maximum post-encounter eccentricity is always $\lesssim 0.8$, in agreement with our statement.

From Figure 6 we note that t_{gw} is longer than t_{hard} , for $a \gtrsim 0.5 - 0.3$ AU. This implies that the lifetime of a binary IMBH is controlled by 3-body scattering on the hardening time t_{hard} , as long as the binary separation $a \sim 0.1$ AU. Therefore, we can neglect the effect of gravitational wave emission, since we consider binaries wider than 0.1 AU.

The expected number of supra-thermal stars is a fraction f of the total number N of stars strongly interacting with a binary IMBH. The latter is given by (cfr. CMP):

$$N = \frac{(M_1 + M_2)}{m \xi_E} \ln \left(\frac{a_0}{a_{st}} \right) \quad (7)$$

where a_0 is the initial semi-major axis of the binary and a_{st} is the minimum semi-major axis for the encounter to give a supra-thermal star. In eq. (7) we impose $a_0 = 2000$ AU, corresponding to the orbital separation below which the binary becomes reasonably hard to generate supra-thermal stars, and $a_{st} = 0.1$ AU, the orbital separation below which

the cross section for 3-body encounters becomes negligible. We then calculate the number of stars that remain bound to the cluster and the number of supra-thermal stars using the statistics derived in our simulations (see the percentages given in Table 3, respectively in first column -for the bound stars- and in fourth column -for the supra-thermal). The results are shown in Table 7. The total number of bound stars is always greater than 400 and the number of stars stirred up to supra-thermal velocities is always greater than 100, even for the lightest system ($M_1 = 50 M_\odot$, $M_2 = 10 M_\odot$).

Supra-thermal stars may be recognized from their proper motion and/or Doppler line shift. Hence we have to take into account projection effects of velocity vectors. These effects depend in turn on the orientation of the angular momentum of the binary IMBH \mathbf{J}_{BH} with respect to the line of sight. We find that about 80% of the supra-thermal stars can be recognized as such in the best case, i.e. when the line-of-sight happens to be nearly parallel to the orbital angular momentum of the binary IMBH \mathbf{J}_{BH} (if we are measuring proper motions) or when the line-of-sight is nearly perpendicular to \mathbf{J}_{BH} (if we are measuring Doppler-shifts). On the contrary, the percentage reduces to about 50% when we are in the most unlucky cases, i.e. when the line of sight happens to be nearly perpendicular to the orbital angular momentum of the binary IMBH \mathbf{J}_{BH} (if measuring proper

Table 7. Number of supra-thermal stars^a

M_1^b	M_2^b	Interacting stars ^c	Bound stars ^d	Supra-thermal stars	Supra-thermal stars (last 2 Gyrs) ^e
50	10	728	467	128	86
50	50	1651	1009	219	146
100	10	2060	1567	238	157
100	50	1722	727	262	158
200	10	1945	1057	306	176

^a These numbers are calculated for binaries having $a_0 = 2000$ AU and $a_{st} = 0.1$ AU

^b In units of solar masses. M_1 and M_2 represent respectively the mass of the more and of the less massive black hole in the binary IMBH.

^c Total number of stars which have an interaction with the binary IMBH.

^d Number of stars which after the interaction remain bound to the cluster.

^e Supra-thermal stars formed in the last 2 Gyrs.

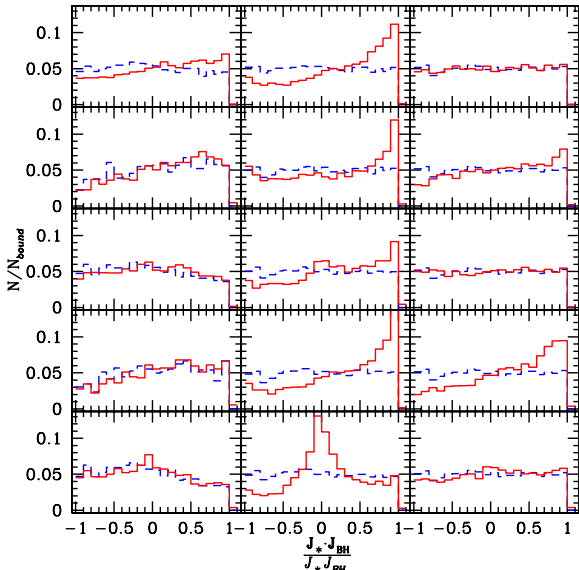


Figure 5. The histograms show the distribution of $\frac{J_* \cdot J_{BH}}{J_{*} J_{BH}}$ for all the considered cases. *Solid line* indicates the distribution after the encounter; *dashed line* indicates the distribution before the encounter. From the up left panel, going toward right: case A2, A3, A4, B2, B3, B4, C2, C3, C4, D2, D3, D4, E2, E3, E4. We do not plot cases A1, B1, C1, D1 and E1 because they are similar to cases A2, B2, C2, D2 and E2. On the y-axis the number of cases for each bin is normalized to the total number of bound stars (N_{bound}).

motions), or when the line of sight is parallel to \mathbf{J}_{BH} (if measuring Doppler shifts). Assuming these percentages, we find that the number of recognizable supra-thermal stars over the entire cluster is ~ 60 -100 for a "light" binary IMBH ($M_1 = 50 M_\odot$, $M_2 = 10 M_\odot$) and ~ 130 -210 for a "moderately massive" binary IMBH ($M_1 = 100 M_\odot$, $M_2 = 50 M_\odot$).

Our calculation refers to all stars, including also compact remnants (neutron stars, white dwarfs) and stellar types which are too faint for allowing a measurement of proper motion or radial velocity. Using the numerical code which will be described in the next Section, we find that the stars with mass from 0.6 to $0.9 M_\odot$ (a mass range which in-

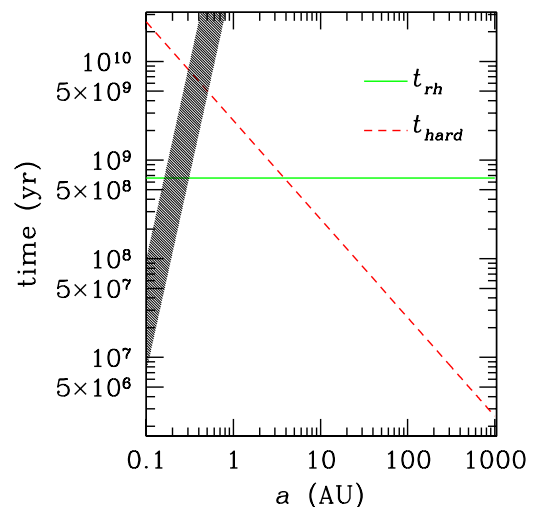


Figure 6. Half mass relaxation time, t_{rh} , and hardening time, t_{hard} , as a function of the initial orbital separation a (in AU) of the binary IMBH, for $n = 10^5 \text{ pc}^{-3}$, $\xi_E = 1$, and $\sigma = 8.5 \text{ km s}^{-1}$. The shadowed area indicates the gravitational wave timescale t_{gw} for binary IMBHs in the considered range of masses (from 60 to $210 M_\odot$) and with eccentricity $e = 0.7$.

cludes red giant (RGB), horizontal branch (HB) and bright enough main sequence (MS) stars) represent about the 45% of the stars enclosed within² $0.1 r_c$ of a GC like NGC 6752. This means that, in the case of a binary of $(100 M_\odot, 50 M_\odot)$, we are able to recognize only 50-100 supra-thermal stars.

There is a further problem concerning the number of surviving supra-thermal stars. Nearly all the proposed mechanisms of formation of binary IMBHs in GCs (Miller & Hamilton 2002; Sigurdsson & Hernquist 1993) predict that such binaries are born within the first Gyr since the forma-

² We consider the region within $0.1 r_c$, because we are interested in those stars which have the highest probability of interacting with the central binary IMBH.

tion of the GC itself. If this is true, considering the hardening time t_{hard} plotted in Figure 6, the binary IMBHs which still survive today must have orbital separation $\lesssim 1$ AU (for a cluster with $n = 10^5$ pc $^{-3}$). This means that all the supra-thermal stars produced when the binary had orbital separation $a \gtrsim 3$ AU have already been thermalized, because a time much longer than t_{rh} has elapsed (Fig. 6). Then, we can observe only the supra-thermal stars produced in the last ~ 2 Gyr (about $3 t_{rh}$, because a supra-thermal star can have apo-center distance larger than the half mass radius and, therefore, relaxation time longer than t_{rh}). Luckily, the orbital separation of a IMBH binary remains in the range 0.1-3 AU for a long time, because the hardening rate is lower for such a hard binary, and a large fraction of supra-thermal stars ($\sim 60\%$) is produced in this stage. The number of these "surviving" supra-thermal stars is reported in Table 7, 6th column. Let us consider again the IMBH binary of (100,50) M_\odot . The total number of supra-thermal stars produced by this binary in the last 2 Gyrs is ~ 160 . This means that, taking into account projection effects and considering only bright enough stars (i.e. in the mass range 0.6 - $0.9 M_\odot$), we are finally left with only 30-60 recognizable supra-thermal stars.

In this discussion we have not considered the effective instrumental errors so far. We now briefly report on them, without entering in details. Even if STIS is no more operative, its accuracy remains a good lower limit for future spectrographs. Observing with STIS stars in a globular cluster with distance from the Sun of the order of 4-10 kpc, one can expect an error of 1-2 km s $^{-1}$ in the determination of radial velocity. For example, van der Marel et al (2002), reported spectra of about 130 stars in the core of M15 (distance from the Sun about 10 kpc) with an observational error of the order of 1.3 km s $^{-1}$. A somewhat higher error can be estimated for proper motion measurements with the HST/WFPC2. Drukier et al. (2003) combined two sets of observations with the WFPC2 (one taken in 1994, the second in 1999) for a sample of 1281 stars in NGC 6752, estimating a median error of 0.31 mas yr $^{-1}$ with a mode of 0.17 mas yr $^{-1}$. For the distance of NGC 6752 this means a median error of ~ 6 km s $^{-1}$ with a mode of ~ 3 km s $^{-1}$, which is still an acceptable accuracy to distinguish supra-thermal stars. Similar considerations hold for HST/ACS (see e.g. Anderson 2002; Anderson & King 2003). Since we defined supra-thermal the stars with projected velocity higher than ~ 12 km s $^{-1}$ (16 km s $^{-1}$ for proper motion measurements), an error of 1-2 km s $^{-1}$ (3-6 km s $^{-1}$ for proper motion measurements) is sufficient to distinguish supra-thermal from other cluster stars, in clusters like NGC 6752. In summary, the main problem in detecting supra-thermal stars is not the error on the single measurement but the possibility of observing a sufficient large sample of stars, since supra-thermal stars are expected to be a very small fraction of cluster stars.

4.2 Spatial distribution of the supra-thermal stars

Since supra-thermal stars are only few tens, the possibility of recognizing them may be significantly enhanced if their radial distribution shows some characteristic feature. Thus, it is of interest to study how supra-thermal stars evolve in the cluster and what is their radial distribution.

To this purpose we have explored the dynamics of

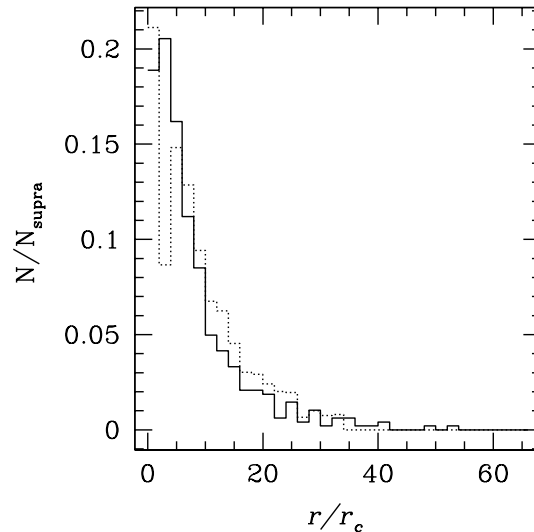


Figure 7. Final projected distribution of the high velocity supra-thermal stars (solid line) in the case D3. The peak is at $3 r_c$. On the y-axis the number of cases for each bin is normalized to the total number of supra-thermal stars. The (dotted line) shows the radial distribution of red giant stars in NGC 6752 (normalized to the total number of red giant stars in the sample).

supra-thermal stars in a cluster under the action of dynamical friction and the influence of two-body relaxation effects using an updated version of the code described in Sigurdsson & Phinney 1995. The code first generates a cluster background model, i.e. a multi-mass King density profile which in our case reproduces that of NGC 6752, and we inject in this background supra-thermal stars whose initial positions and velocities are those obtained by our 3-body simulations. We followed the dynamical evolution of these stars for a random time t uniformly distributed in the range $0 < t \leq 3 t_{rh}$. In this way we can see how supra-thermal distribute in the cluster before thermalization. After evolution for a time $t \lesssim 3 t_{rh}$ we select the stars that still are supra-thermal. We applied this procedure to the cases D1, D2, D3 and D4.

The stars which were still supra-thermal when the simulation stopped and that can be observed as supra-thermal, taking into account two-dimensional (one-dimensional) projection effects and ejections, are about 70% (60%) of the initial sample. These stars present a radial distribution like that shown in Figure 7 (for the case D1). This distribution is peaked around a radius r_{peak} which is of the order of few core radii for all the considered systems. For a binary IMBH with $M_1 = 100 M_\odot$, $M_2 = 50 M_\odot$ and $a = 1$ AU (D1) $r_{peak} = 3 r_c$ and we have calculated that it is enough to measure radial velocities within a distance of $6 r_c$ from the cluster center, in order to avoid poissonian fluctuations to smear out the peak.

Taking again into account both projection effects and luminosity criteria, only ~ 30 supra-thermal stars are located within $6 r_c$. We found that, if the velocity distribution is Maxwellian, ~ 10 stars with velocity in the supra-thermal range are predicted to inhabit within a distance of $6 r_c$ from the center of NGC 6752. Then, the number of supra-thermal

stars produced by interactions with a binary IMBH prevails on the high velocity tail of the Maxwellian distribution. On the other hand the presence of this tail further dilutes the signature of supra-thermal stars.

In Fig. 7 we have finally compared the radial distribution of 1984 red giant stars (dotted line) observed in NGC 6752 (591 of them from HST/WFPC2 observations, 1393 from the ESO/MPG WFI. See Sabbi et al. 2004) with that calculated for supra-thermal stars (solid line). RGB stars appear to be more concentrated toward the center of the cluster (the maximum being between 0 and 2 r_c); but the two distributions are quite similar.

4.3 Detectability of angular momentum alignment

We now discuss the observability of the signature of the angular momentum alignment effect. Column 2 of Table 4 tells us that in the most favorite case about 70% of the stars which remain bound are corotating with the binary IMBH, whereas 30% are counterrotating. This means that, if there is a binary IMBH of $M_1 = 100 M_\odot$ and $M_2 = 50 M_\odot$, we should have about 90-150 corotating and only 40-60 counterrotating supra-thermal stars. On the other hand, angular momentum alignment effects are visible only for sufficiently wide binaries ($a > 10$ AU). Thus, unless a binary IMBH is formed recently in a cluster, the alignment effect today is completely washed out by dynamical friction.

However, we notice that a very low probability mechanism of binary IMBH formation in GCs in recent epochs exists. In fact, there is some possibility that a "last single BH" (Sigurdsson & Hernquist 1993), ejected from the core in the early stages of the GC life, remains in the halo for several Gyrs. The relaxation timescale out in the halo is long, and if the orbits can circularize there (maybe due to time varying galactic tidal field), then the return time to the core is long. When this BH comes back to the core, there is a high probability that it forms a binary with the central IMBH. Such a binary IMBH would be originated in late epochs. However, the probability for this process to occur is low, because it requires the BH to receive just the fine-tuned post-encounter velocity needed to remain in the outer halo: if the velocity is slightly too high, the BH will be ejected from the entire cluster; whereas, if the velocity is low, the return time to the core will be too short.

The process described here is an unmistakable feature of a binary IMBH, which can not be produced by a distribution of stellar binaries interacting via 3-body encounters with cluster stars. Instead, we need dedicated 3-body simulations to check whether even stellar binaries can produce effects like those described in §3.1 and §4.2.

5 SUMMARY

In our work we explored the effects that the presence of a binary IMBH imprints on the velocity and angular momentum of cluster stars, due to 3-body encounters with it. The main results of our analysis can be summarized as follows.

(i) A binary IMBH generates a family of supra-thermal stars, i.e. of stars which remain bound to the cluster, but have a velocity higher than the dispersion velocity. (§ 3.1).

(ii) A fraction of stars tend to align their angular momentum, \mathbf{J}_* , with that of the binary IMBH, \mathbf{J}_{BH} . This fraction depends on the reduced mass μ and on the semi-major axis a of the binary IMBH, but it is always of the order of 55-70%. This means that the angular momentum distribution of stars that have suffered 3-body interaction with a binary IMBH presents a slight anisotropy (§ 3.2).

(iii) The present theoretical models of binary IMBH formation indicate that these systems are produced in the first Gyr of the GC life. This means that today, in dense clusters like NGC 6752, binary IMBHs have, due to hardening, orbital separation $a \lesssim 1$ AU. As a consequence, supra-thermal stars produced when the binary was wider (more than 2 Gyrs ago for the case of NGC 6752) have now already thermalized. That reduces the current population of residual supra-thermal stars about of a factor two with respect to the total population produced during the entire IMBH lifetime (§ 4.1). On the other hand these "surviving" supra-thermal stars do not show any signature of angular momentum alignment (§ 4.3), because this effect is evident only when the stars interact with a relatively wide binary ($a > 10$ AU).

(iv) How many supra-thermal stars are expected to be produced by a binary IMBH and still surviving in a GC like NGC 6752? We estimated few hundreds of supra-thermal stars. Once subtracted the fraction of compact remnants and faint stars and taking into account projection effects and thermalization of the oldest supra-thermal stars (see §4.1) we calculate that there may be at most few tens of supra-thermal stars suitable to be recognized as such in the whole cluster. It can be interesting to notice that there is already a claim for the detection of high velocity stars in 47 Tuc (Meylan, Dubath & Mayor 1991).

(v) Given the aforementioned relatively small number of expected supra-thermal stars it is important to study their spatial distribution in order to improve the chances of recognizing their origin. To this purpose (see § 4.2), we followed the dynamical evolution of supra-thermal stars in the cluster potential (assuming a cluster model which reproduces the observational characteristics of NGC 6752), taking into account dynamical friction and two body relaxation. We found that, before thermalization, supra-thermal stars tend to cluster within 6 r_c .

(vi) Although we have not performed a detailed simulation of the observability of the few tens of expected supra-thermal stars with present detectors, simple considerations (see §4.1 and §4.2) suggest that the various observational biases (mainly related with the limited field-of-view of the most sensitive instruments) may lead to the detection of only a sub-sample of the population.

In the light of these findings, the search of supra-thermal stars and of anisotropies in their angular momentum distribution can hardly provide useful indications on the existence of binary IMBHs in GCs with present instruments. However, it may become a feasible task for future instruments having much bigger collecting area and equipped with detectors having much larger field of view, like (Gilmozzi 2004) the Thirty Meter Telescope (TMT) or the OverWhelmingly Large Telescope (OWL).

6 ACKNOWLEDGMENTS

We thank Francesco Ferraro for useful discussions on the issue of supra-thermal star detection. We also thank Marc Freitag, Cole Miller and the anonymous Referee for a critical reading of the manuscript. This work found first light during the workshop "Making Waves with Intermediate-Mass Black Holes" (20-22 May 2004, Penn State University). M. C. and M. M. acknowledge the Center for Gravitational Wave Physics for kind hospitality. S. S. acknowledges support by the Center for Gravitational Wave Physics funded by the NSF under cooperative agreement PHY 01-14375 and NSF grant PHY 02-03046. M. C. and A. P. acknowledge financial support from the MURST, under PRIN03.

REFERENCES

Abel T., Bryan G. L., Norman M. L., 2002, *Sci*, 295, 93

Anderson J., The 2002 HST Calibration Workshop : Hubble after the Installation of the ACS and the NICMOS Cooling System, Proceedings of a Workshop held at the Space Telescope Science Institute, Baltimore, Maryland, October 17 and 18, 2002. Edited by Santiago Arribas, Anton Koekemoer, and Brad Whitmore, 2002, 13

Anderson J., King I. R., 2003, *AJ*, 126, 772

Bassa C. G., Verbunt F., van Kerkwijk M. H., Homer L., 2003, *A&A*, 409, 31

Baumgardt H., Hut P., Makino J., McMillan S., Portegies Zwart S., 2003a, *ApJL*, 582, 21

Baumgardt H., Makino J., Hut P., McMillan S., Portegies Zwart S., 2003b, *ApJL*, 589, 25

Belczynski K., Bulik T., Rudak B., 2004, *ApJL*, 608, 45

Camilo F., Rasio F. A., 2005, ASP Conf. Ser. Vol. 328, 2005: Binary Radio Pulsars, eds. F. A. Rasio, I. H. Stairs, astro-ph/0501226

Colpi M., De Vecchi B., Mapelli M., Patruno A., Possenti A., 2005, astro-ph/0504198, Invited review in: "Interacting binaries", July 4-10 Cefalu, eds. Antonelli et al., to be published with AIP

Colpi M., Mapelli M., Possenti A., 2004, Coevolution of Black Holes and Galaxies, from the Carnegie Observatories Centennial Symposia. Carnegie Observatories Astrophysics Series. Edited by L. C. Ho, 2004. <http://www.ociw.edu/ociw/symposia/series/symposium1/proceedings.html>

Colpi M., Mapelli M., Possenti A., 2003, *ApJ*, 599, 1260

Colpi M., Possenti A., Gualandris A., 2002, *ApJL*, 570, 85

D'Amico N., Possenti A., Fici L., Manchester R. N., Lyne A. G., Camilo F., Sarkissian J., 2002, *ApJL*, 570, 89

Drukier G. A., Bailyn C. D., Van Altena W. F., Girard T. M., 2003, *AJ*, 125, 2559

Dubath P., Meylan G., Mayor M., 1997, *A&A*, 324, 505

Duncan M. J., Shapiro S. L., 1982, *ApJ*, 253, 921

Fabbiano G., 2004, Compact Binaries in the Galaxy and Beyond, Proceedings of the conference held 17-22 November, 2003 in La Paz, Baja California Sur. Edited by G. Tovmassian and E. Sion. Revista Mexicana de Astronomia y Astrofisica (Serie de Conferencias) Vol. 20. IAU Colloquium 194, pp. 46-49

Ferraro F. R., Possenti A., Sabbi E., D'Amico N., 2003b, *ApJL*, 596, 211

Ferraro F. R., Possenti A., Sabbi E., Lagani P., Rood R. T., D'Amico N., Origlia L., 2003a, *ApJ*, 595, 179

Fregeau J. M., Cheung P., Portegies Zwart S. F., Rasio F. A., 2004, *MNRAS*, 352, 1

Freitag M., Rasio F. A., Baumgardt H., 2005a, astro-ph/0503129

Freitag M., Gürkan M. A., Rasio F. A., 2005b, astro-ph/0503130

Gebhardt K., Pryor C., Williams T. B., Hesser J. E., 1995, *AJ*, 110, 1699

Gebhardt K., Pryor C., Williams T. B., Hesser J. E., Stetson P. B., 1997, *AJ*, 113, 1026

Gebhardt K., Pryor C., O'Connell R. D., Williams T. B., Hesser J. E., 2000, *AJ*, 119, 1268

Gebhardt K., Rich R. M., Ho L. C., 2002, *ApJL*, 578, 41

Gebhardt K., Rich R. M., Ho L. C., 2005, accepted for publication in *ApJ*

Gerssen J., van der Marel R. P., Gebhardt K., Guhathakurta P., Peterson R. C., Pryor C., 2003, *AJ*, 125, 376

Gerssen J., van der Marel R. P., Gebhardt K., Guhathakurta P., Peterson R. C., Pryor C., 2002, *AJ*, 124, 3270

Gilmozzi R., 2004, *SPIE*, 5489, in press

Gultekin K., Miller M. C., Hamilton D. P., 2004, *ApJ*, 616, 221

Gürkan M. A., Freitag M., Rasio F. A., 2004, *ApJ*, 604, 632

Heger A., Fryer C. L., Woosley S. E., Langer N., Hartmann D. H., 2003, *ApJ*, 591, 288

Heggie D. C., 1975, *MNRAS*, 173, 729

Hills J. G., 1975, *AJ*, 80, 809

Hills J. G., 1990, *AJ*, 99, 979

Hut P., Bahcall J. N., 1983, *ApJ*, 268, 319

Kulkarni S. R., Hut P., McMillan S., 1993, *Natur*, 364, 421

Madau P., Rees M. J., 2001, *ApJL*, 551, 27

Marchant A. B., Shapiro S. L., 1979, *ApJ*, 234, 317

Marchant A. B., Shapiro S. L., 1980, *ApJ*, 239, 685

Meylan G., Dubath P., Mayor M., 1991, *ApJ*, 383, 586

Miller M. C., 2002, *ApJ*, 581, 438

Miller M. C., Hamilton D. P., 2002, *MNRAS*, 330, 232

Mushotzky R., 2004, *Progress of Theoretical Physics Supplement*, 155, 27

Orosz J. A., 2003, astro-ph/0209041, invited talk at IAU Symp. 212, "A Massive Star Odyssey, from Main Sequence to Supernova", to appear in the proceedings (K. A. van der Hucht, A. Herrero, & C. Esteban eds., San Francisco: ASP)

Peters P. C., 1964, *Phys. Rev.* B136, 1224

Phinney E. S., 1993, Structure and Dynamics of Globular Clusters. Proceedings of a Workshop held in Berkeley, California, July 15-17, 1992, to Honor the 65th Birthday of Ivan King. Editors, S.G. Djorgovski and G. Meylan; Publisher, Astronomical Society of the Pacific, Vol. 50, San Francisco, California

Portegies Zwart S. F., 2004, astro-ph/0406550, Lecture note to appear in "Joint Evolution of Black Holes and Galaxies" of the Series in High Energy Physics, Cosmology and Gravitation. IOP Publishing, Bristol and Philadelphia, 2005, eds M. Colpi, V. Gorini, F. Haardt and U. Moschella ...

Portegies Zwart S. F., Baumgardt H., Hut P., Makino J., McMillan S. L. W., 2004, *Natur*, 428, 724

Portegies Zwart S. F., McMillan S. L. W., 2002, *ApJ*, 576, 899

Portegies Zwart S. F., McMillan S. L. W., 2000, *ApJL*, 528, 17

Possenti A., 2003, Radio Pulsars, ASP Conference Proceedings, Vol. 302. Held 26-29 August 2002 at Mediterranean Agro-nomic Institute of Chania, Crete, Greece. Edited by Matthew Bailes, David J. Nice and Stephen E. Thorsett. San Francisco: Astronomical Society of the Pacific

Quinlan G. D., 1996, *NewA*, 1, 35

Ransom S. M., Hessels J. W. T., Stairs I. H., Freire P. C. C., Camilo F., Kaspi V. M., Kaplan D. L., 2005, *Sci*, 307, 892

Sabbi E., Ferraro F. R., Sills A., Rood R. T., 2004, *ApJ*, 617, 1296

Schneider R., Ferrara A., Natarajan P., Omukai K., 2002, *ApJ*, 571, 30

Shapiro S. L., 1977, *ApJ*, 217, 281

Shapiro S. L., 1985, Proceedings of the Symposium "Dynamics of star clusters", Dordrecht, D. Reidel Publishing Co., 1985, 373

Shapiro S. L., Marchant A. B., 1978, 225, 603

Sigurdsson S., Hernquist L., 1993, *Natur*, 364, 423
 Sigurdsson S., Phinney E. S., 1995, *ApJS*, 99, 609
 Sigurdsson S., Phinney E. S., 1993, *ApJ*, 415, 631
 van der Marel R. P., 2004, *Coevolution of Black Holes and Galaxies*, from the Carnegie Observatories Centennial Symposia. Published by Cambridge University Press, as part of the Carnegie Observatories Astrophysics Series. Edited by L. C. Ho
 van der Marel R. P., Gerssen J., Guhathakurta P., Peterson R. C., Gebhardt K., 2002, *AJ*, 124, 3255
 Volonteri M., Haardt F., Madau P., 2003, *ApJ*, 582, 559

APPENDIX A: CHOICE OF IMPACT PARAMETERS

We chose impact parameters in order to select all the interactions which have not negligible energetic exchange (about $\Delta E_{\text{BH}}/E_{\text{BH}}^{\text{in}} \gtrsim 10^{-3}$), to allow a complete coverage of all the interactions that enter in the supra-thermal domain (20-40 km s⁻¹). We used the formula of the gravitational focusing (Sigurdsson & Phinney 1993), for which

$$b_{\text{max}} \sim \left(\frac{2G M_T p}{v_{\infty}^2} \right)^{1/2}, \quad (\text{A1})$$

where b_{max} is the maximum impact parameter, M_T the total mass of the binary, v_{∞} the relative velocity at infinity and p the distance of closest approach.

We firstly imposed $p \sim (10a)$ for all the systems (where a is the semi-major axis of the binary). Then we made some test-run to check what were the best maximum impact parameters to include all the strongly interacting stars (and then the supra-thermal stars). The results of these checks induced us to slightly modify b_{max} as calculated with eq. (A1). In fact, when a binary has a very large semi-major axis (case with $a=100$ or 1000 AU), the choice $p \sim (10a)$ means that the incoming star will pass very far from the center of mass of the binary, will interact very weakly with the binary (unless it closely approaches the secondary component of the binary itself) and never obtain $\Delta E_{\text{BH}}/E_{\text{BH}}^{\text{in}} > 10^{-3}$. The velocity at infinity peak is always $\ll 10$ km/s.

On the other hand, when the binary has a very small semi-major axis ($a \leq 1$ AU), the choice $p \sim (10a)$ does not take into account all the strong interactions. In fact all the stars which have $p \sim (10a)$ pass so closely to the very hard binary to become very fast (> 100 km/s). But, if we consider only $p \sim (10a)$, we miss most of the interacting stars. In fact, if we take $p \sim (50-100)a$, we still have stars that sufficiently approach to the center of mass of the binary to receive an outgoing velocity $\sim 20-40$ km/s (exactly the range of supra-thermal stars). And, statistically, stars with $p > 10a$ will be much more numerous than stars with $p < 10a$. Then, if we take $p \lesssim (10a)$, we miss the bulk of interacting stars belonging to the supra-thermal interval.

Then, both when we choose a small b_{max} ($p \lesssim 10a$) for a very hard binary and a large b_{max} ($p \gtrsim 10a$) for a wide binary, we introduce a bias. In the former case we select only high velocity encounters ($\Delta E_{\text{BH}}/E_{\text{BH}}^{\text{in}} \gg 10^{-3}$), omitting the bulk of interacting stars; in the latter we risk to consider also unperturbing flybys ($\Delta E_{\text{BH}}/E_{\text{BH}}^{\text{in}} \ll 10^{-3}$).

Fig. A1 represents the post-encounter asymptotic velocity distribution of the star in the case of a binary with $M_1=50 M_{\odot}$, $M_2=10 M_{\odot}$, $a=100$ AU. The dotted line shows

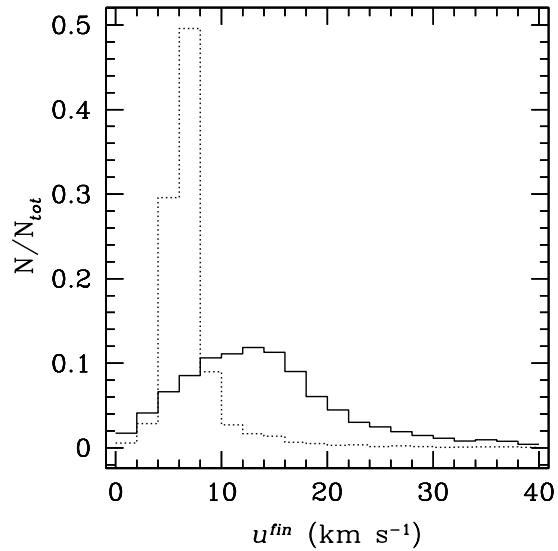


Figure A1. Post-encounter asymptotic velocity distribution of the star, after the interaction with a binary of $M_1=50 M_{\odot}$, $M_2=10 M_{\odot}$, $a=100$ AU. The solid line shows the case with $b_{\text{max}}=100$ AU (the runs reported in the paper as case A3), whereas the dotted line shows a case with $b_{\text{max}}=2000$ AU (corresponding to adopt $p = 10a$ in eq. (A1)). On the y-axis the number of cases for each bin is normalized to the total number of resolved runs (N_{tot}).

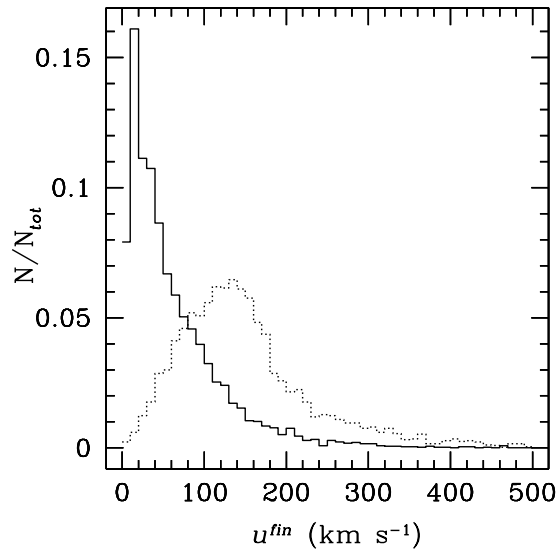


Figure A2. Post-encounter asymptotic velocity distribution of the star after the interaction with a binary of $M_1=50 M_{\odot}$, $M_2=10 M_{\odot}$, $a=1$ AU. The solid line shows the case with $b_{\text{max}}=60$ AU (the runs reported in the paper as case A1), whereas the dotted line shows a case with $b_{\text{max}}=1$ AU (corresponding to impose $p = 1a$ in eq. (A1)). On the y-axis the number of cases for each bin is normalized to the total number of resolved runs (N_{tot}).

the case with $b_{max}=2000$ AU (corresponding to adopt $p = 10a$ in eq. (A1)): most of interactions are very weak flybys (velocity < 8 km/s), and we cannot count them as strong interactions. Instead, the solid line shows the case with $b_{max}=100$ AU ($p = a$), i.e. the runs reported in the paper as case A3: this represents a valid statistic sample of all the strong interactions (the peak being at ~ 13 km/s). On the other hand, Fig. A2 shows the post-encounter asymptotic velocity distribution of the star in the case of a binary with $M_1=50 M_\odot$, $M_2=10M_\odot$, $a=1$ AU. The dotted line, showing the case with $b_{max}=1$ AU (corresponding $p = 1a$), is peaked at very high velocities. Instead, the solid line, for $b_{max}=60$ AU (case A1), shows that, if we take into account also encounters with $p > 1a$, but still with $\Delta E_{BH}/E_{BH}^{in} > 10^{-3}$, we have a very different velocity distribution, peaked at 20-30 km/s. We think that the last one is the only statistically significant case, because it takes into account all the interacting stars with significant energetic exchange. The dotted line, instead, misses the most numerous class of interactions.

For these reasons we adopted new criteria for the choice of p (to be substituted in eq. A1 to derive b_{max}) as:

- if $a \geq 100$ AU, then $p \sim a$;
- if $1 \text{ AU} < a < 100 \text{ AU}$, then $p \sim (10a)$;
- if $a=1$ AU, then $p \sim (60 - 100) a$.

This means, that our selected maximum impact parameter is quite constant (~ 100 AU), independent of the semi-major axis a of the binary (at least if $a < 1000$ AU).

We think that the big maximum impact parameter required by systems with $a=1$ AU is due to the uncommonly large mass ratio between the binary and the incoming star. In fact, when at least one of the two components of the binary is so massive, it plays an important role on the gravitational focusing, nearly independently of the semi-major axis. Then, the incoming star is attracted toward the center of mass of the binary, even if it starts with very large impact parameter. But a binary of $a=1$ AU has a very small geometrical cross-section; then only a very small fraction of interacting stars will have an effective pericenter $p \leq a$. Thus, only a few stars will interact very strongly with the binary. Most of the stars will have a pericenter $p > a$; but the binary has a so large binding energy that also these stars receive non-negligible post-encounter velocity, and they can become supra-thermal.

Even the behavior of ξ_E shown in Fig. 2, apparently different from what predicted by the Heggie's law when $a=1$ AU, depends on our choice of b_{max} . In fact, if for a binary with semi-major axis $a = 1$ AU we choose $p \sim a$ (corresponding to $b_{max} \sim 1$ AU, instead of 60-100 AU), we obtain $\xi_E \sim 4$, higher than the value of ξ_E derived for wider binaries and in agreement with Heggie's law. On the other hand, we need to select $p \gg a$, because we want to include all the interactions which have not negligible energetic exchange. But this choice lowers the average value of ξ_E from 4 to about 1.